

XReal: Realistic Anatomy and Pathology-Aware X-ray Generation via Controllable Diffusion Model

Anees Ur Rehman Hashmi¹, Ibrahim Almakky¹, Mohammad Areeb Qazi¹,
Santosh Sanjeev¹, Vijay Ram Papineni², Dwarikanath Mahapatra³, and
Mohammad Yaqub¹

¹ Mohamed bin Zayed University of Artificial Intelligence, Abu Dhabi, UAE
`{firstname.secondname}@mbzuai.ac.ae`

² Sheikh Shakhboub Medical City, Abu Dhabi, UAE

³ Inception Institute of Artificial Intelligence, Abu Dhabi, UAE

Abstract. Large-scale generative models have demonstrated impressive capacity in producing visually compelling images, with increasing applications in medical imaging. However, they continue to grapple with the challenge of image hallucination and the generation of anatomically inaccurate outputs. These limitations are mainly due to the sole reliance on textual inputs and lack of spatial control over the generated images, hindering the potential usefulness of such models in real-life settings. We present XReal, a novel controllable diffusion model for generating realistic chest X-ray images through precise anatomy and pathology location control. Our lightweight method can seamlessly integrate spatial control in a pre-trained text-to-image diffusion model without fine-tuning, retaining its existing knowledge while enhancing its generation capabilities. XReal outperforms state-of-the-art x-ray diffusion models in quantitative and qualitative metrics while showing 13% and 10% anatomy and pathology realism gain, respectively, based on the expert radiologist evaluation. Our model holds promise for advancing generative models in medical imaging, offering greater precision and adaptability while inviting further exploration in this evolving field. A large synthetically generated data with annotations and code is publicly available at <https://github.com/BioMedIA-MBZUAI/XReal>.

Keywords: Diffusion Model · Clinical Realism · Image Generation · X-ray

1 Introduction

Deep generative models have shown remarkable success in a wide range of applications, including healthcare, with the ability to generate high-quality text and images with intricate details [30, 3, 32]. However, despite significant advancements in image quality, these models frequently struggle with hallucinations,

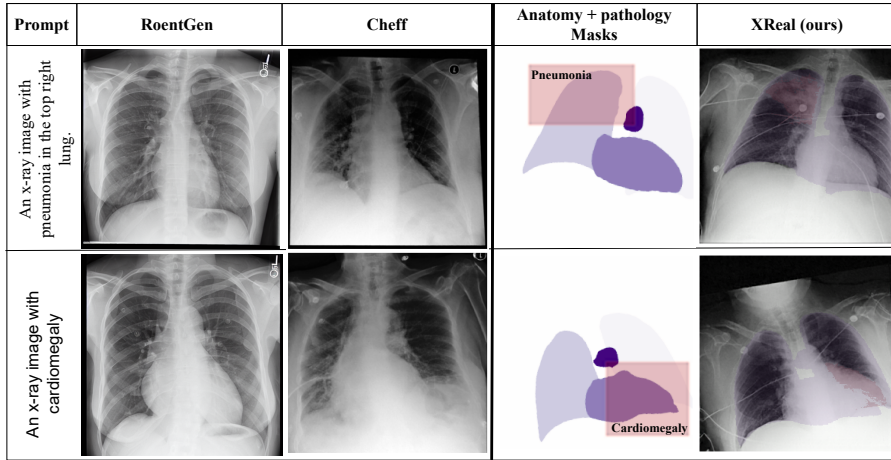


Fig. 1. X-ray generation using different diffusion models. Text-to-image models (RoentGen [6] and Cheff [36]) struggle to follow the pathology location information specified in the prompts and do not offer any anatomy control. Our proposed XReal model produces clinically realistic X-ray images with precise control over the anatomy and pathology manifestation (red overlaid mask).

often leading to the generation of images containing illogical and unrealistic content [31]. One primary factor contributing to this challenge is their reliance solely on textual input for conditioning, which often falls short of providing complete guidance for logical and realistic image generation [2,4].

Text-to-image generative models, including Variational AutoEncoder (VAEs) [20], Generative Adversarial Networks (GANs) [14], and more recently, diffusion models [11] have shown promising generative capabilities for high-quality image synthesis in the medical domain [15,6,36]. However, relying solely on free-form text to generate images [6,36] limits the control over critical spatial information in medical images, especially surrounding anatomical structures and pathology manifestations (Fig. 1). This absence of control over the relative location of organs and diseases ignores that many diseases are plausible only when they are manifested in a specific location relative to the organs of interest in the body. This concern is further amplified in chest X-ray images, where a given disease can manifest in many regions, and minor alterations to its manifestation can significantly impact the disease identification and overall image interpretation. This limits the applications for such models in radiologist training and for counterfactual diagnosis [8,15].

GANs have been a popular method for generating X-ray images [33,25,7,39]. However, GAN-based approaches face training stability challenges and lack image diversity. More recently, [5] employed a stable diffusion model [32] to generate X-ray images from radiology reports. Similarly, [36] developed a cascaded Latent-Diffusion Model (LDM) for x-ray generation from reports, incorporating

text-image generation and resolution enhancement diffusion models. [27] focused on generating class-conditional X-ray images while employing privacy-enhancing sampling strategies during image generation. Although textual conditioning or class labels for generating X-ray images remain active research areas, the utilization of spatial information, particularly concerning X-ray pathologies, remains largely unexplored.

Different perspectives have been considered in addressing spatial control within diffusion models applied to natural scene images. The first perspective focuses on training task-specific diffusion models using paired masks and images [23,24,38,13]. Another perspective is to manipulate the cross-attention layers in pre-trained diffusion models [28,37,10], making them sensitive to textual inputs and often causing a drop in image quality. Hypernetworks, first explored with GANs [1,12,22] for style-transfer and image editing, have also been integrated with diffusion models, where [40] introduced ControlNet and fine-tuned a diffusion model’s encoder as a hypernetwork for spatial guidance. In the medical domain, previous attempts for spatial control have focused on ultrasound imaging, with [34] generating 2D echocardiograms. More recently, [35] introduced a method for echocardiography video synthesis given a semantic segmentation mask. Furthermore, [21] introduced anatomical control in MRI and CT slices by concatenating the input masks to diffusion model channels in each timestep. However, no prior research has been done on enhancing medical realism by exerting spatial control over anatomy and pathology in generated images, particularly in the context of chest X-ray generation, despite its widespread applications.

To address this challenge, we introduce XReal, a diffusion model capable of generating high-quality, clinically realistic X-ray images given anatomy and pathology masks to control the organs’ location, size, shape, and manifestation of the pathology. Through spatial control, our lightweight model can generate clinically relevant and anatomically coherent X-ray images, enhancing the usefulness of the generated data for downstream medical applications. To this effect, the main contributions of this work are as follows:

- We introduce XReal, a novel pathology and anatomy-aware controllable diffusion model for realistic X-ray image generation. XReal can generate high-quality, clinically realistic X-ray images with precise control over the organs’ location, size, and shape, as well as the manifestation of the pathology.
- We present the image editing and pathology location interpolation capabilities of XReal. We also use XReal to create a clinically validated synthetic publicly available X-ray dataset, *BiomedCXR*, containing paired images, anatomical masks, and pathology annotations.
- We conduct extensive experiments, comparing XReal with existing image generation models and demonstrate state-of-the-art performance in quantitative metrics and expert radiologist evaluation.

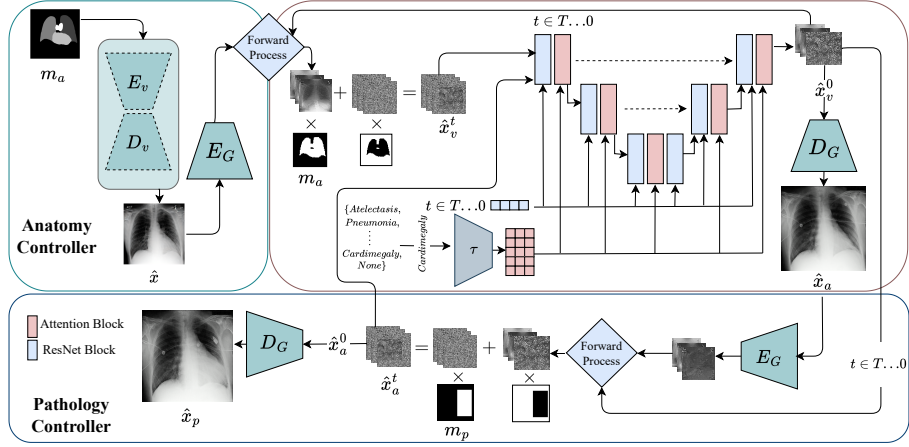


Fig. 2. XReal uses a two-stage process: (Top) Generating image \hat{x}_a from anatomy mask m_a via a lightweight VAE in the Anatomy Controller, and (2) infusing pathology p into \hat{x}_a at m_p to obtain the final image \hat{x}_p .

2 Method

We propose XReal, where the aim is to generate an image \hat{x}_p given an anatomy mask m_a , a pathology mask m_p , and the pathology label $p \in P$, where $P = \{p_1, \dots, p_n\}$ is the set of n possible pathologies. The generated image \hat{x}_p should follow the anatomical structure specified in m_a while manifesting the pathology p in the specified location within m_p . As depicted in Fig. 2, XReal consists of the Anatomy Controller component followed by a latent diffusion model and the Pathology Controller.

Anatomy Controller. To control the anatomical structure within \hat{x}_p , we propose an Anatomy Controller consisting of a VAE having encoder E_v and decoder D_v trained to learn $\hat{x} = D_v(E_v(m_a))$, where $\hat{x} \approx x$ and (x, m_a) are an input X-ray image and its corresponding anatomy mask, respectively. We use the spatial information present in the VAE latent space and apply anatomical guidance directly to the latent image representation. The image \hat{x} carries the overall anatomical structure as provided in m_a ; however, it does not contain any X-ray image details and may contain artefacts. Following this, a different VAE encoder E_G from the latent diffusion model (LDM) encodes \hat{x} as latent \hat{x}_v ($\hat{x}_v = E_G(\hat{x})$), which is passed to the diffusion model G to generate \hat{x}_v^0 . Before passing \hat{x}_v through G , we infuse it with m_a . In other words, we first add a specific amount of noise to \hat{x}_v to get \hat{x}_v^t using the forward diffusion process as described in [17]. We compute $\hat{x}_v^t = \hat{x}_v \times m_a + (1 - m_a) \times \epsilon$ to infuse anatomical information into the diffusion model, where ϵ represents the Gaussian noise. This infusion allows G to utilize the anatomical information present in the noisy x_v while generating the peripheries (arms, bones, etc.) using the random Gaussian

noise. Motivated by our empirical analysis, the initial time steps in the denoising process determine the overall structure of the generated image, while later steps enhance the structure. We apply our anatomical guidance for initial s out of T backward diffusion steps. Finally, the LDM’s VAE decoder D_G decodes \hat{x}_v^0 to \hat{x}_a image containing the desired anatomy. A detailed explanation of the Anatomy Controller is provided in the Algorithm 1 given in Appendix A1.

Latent Diffusion Model. Alleviating the computational cost associated with Diffusion Models [17], similarly to LDM [32], we use a pre-trained VAE [20] model consisting of an encoder E_G and decoder D_G and train a text-to-image diffusion model in its latent space. In LDM, E_G first encodes \hat{x} as \hat{x}_v , which is passed to the UNet-based diffusion model G as input along with the pathology p and timestep t . The iterative denoising process is repeated for T steps to generate the latent \hat{x}_v^0 , decoded to the image space using D_G .

Pathology Controller. Given image \hat{x}_a generated by Anatomy Controller, pathology mask m_p and the pathology p , Pathology Controller generates the image \hat{x}_p containing p at m_p while preserving the anatomy m_a in \hat{x}_a . We use the inpainting capabilities of the pre-trained text-to-xray diffusion model G and fill the m_p region in \hat{x}_a with pathology p . We take a similar approach to the one described in Anatomy Controller and first encode \hat{x}_a to the latent space using E_G . Followed by the addition of random Gaussian noise to the specified region in m_p in the noisy \hat{x}_a^t obtained by the forward diffusion process before passing through G . We repeat this iterative masking and denoising process for T timesteps to obtain \hat{x}_a^0 decoded by D_G to the final X-ray image \hat{x}_p . Notably, we apply m_p for all T timesteps, unlike Anatomy Controller, as our goal here is to infuse the detailed pathology, which requires iteration over entire T steps.

3 Experiments

Dataset: Our text-to-image LDM backbone is trained on the X-ray image and text-label pairs of the MIMIC-CXR dataset [19], which is a large collection of 377,110 chest X-ray images and corresponding free-text radiology reports and labels. During training, our model uses over 120,000 Antero-Posterior (AP) view images from the training subset of the dataset, while we used the official test split for evaluating model performance.

Implementation Details: The VAE models within both the LDM and the Anatomy Controller are trained using a downsampling factor of 4 and have the same architecture. For LDM’s VAE, we used the pre-trained weights from [36], which is further fine-tuned with 50 epochs for the Anatomy Controller. The text-to-image LDM model is trained on 256×256 images for 100 epochs with a constant learning rate of 1×10^{-5} and batch size of 8. Furthermore, we used a linear β noise scheduler with range (0.0015, 0.0295) and set $s = 50$ and $s = 100$ for the Anatomy Controller and Pathology Control with $T = 100$, respectively. Our experiments are conducted on two Nvidia RTX A6000 GPUs and implemented using the Pytorch [29] framework.

Table 1. Performance comparison between XReal and SOTA X-ray image generation methods. ControlNet [40] and XReal are the only models offering any spatial control. [‡]We implemented ControlNet [40] using our LDM backbone. We used the MIMIC-CXR test set as real images to set the upper bound for the performance. [†]denotes reproduced results using the same data split (trained on the MIMIC-CXR train set and tested on the test set).

Model	Quantitative Results					Radiologist Scores	
	MS-SSIM [†]	Dice [†]	FID [↓]	F1 [†]	AUC [†]	Anatomy [†]	Pathology [†]
Cheff [†] [36]	0.415	0.5	24.64	0.51	0.64	3.67	3.74
RoentGen [6]	0.386	0.631	82.14	0.55	0.8	<u>4.14</u>	3.68
LDM (Ours)	0.411	0.51	29.76	0.59	<u>0.78</u>	-	-
ControlNet [‡] [40]	<u>0.63</u>	<u>0.835</u>	<u>29.48</u>	0.56	0.74	4.14	<u>3.88</u>
XReal (Ours)	0.701	0.838	55.12	<u>0.57</u>	0.74	4.73	4.44
Real Images	-	-	-	0.61	0.8	4.41	3.88

4 Results

To quantify the realism of generated data, we use a combination of different evaluation metrics, including the multi-scale structural similarity index measure (MS-SSIM), Dice score (for anatomy control evaluation), classification metrics, and expert radiologist evaluation. Natural image generative models are commonly assessed using the Frechet Inception Distance (FID) [16] to gauge the fidelity of the generated images. FID compares the distribution of generated and real datasets using a pre-trained Imagenet model. However, this does not accurately reflect the generated data’s medical realism, rendering it unsuitable for medical applications. This is reflected in Fig. A2.1 of appendix A2, where images with significant artefacts are given lower FID scores, highlighting the weakness of FID in assessing medical image generation quality.

In Table 1, we present the classification performance, namely F1 and AUC, calculated using the DenseNet-121[18] trained on the MIMIC-CXR dataset. The table also presents the dice score from a pre-trained anatomy segmentation model from the TorchXRayVision library [9] for lung, heart, and aorta segmentation and structural similarity scores (MS-SSIM). We compare our methods with state-of-the-art (SOTA) text-to-image diffusion models. Our text-to-xray LDM backbone outperforms report-to-xray models, namely Cheff [36] and Roentgen [6], in terms of F1 and Area Under the Curve (AUC) scores, suggesting that the report-to-xray diffusion model does not lead to higher performance concerning the accurate manifestation of pathologies.

We assess anatomical realism and control over the organs in the generated dataset using the anatomy segmentation model. To this end, we compare our methodology against ControlNet [40], trained on identical data splits. Table 1 shows that XReal outperforms ControlNet with only 55M parameters compared to ControlNet’s 217M parameters. Furthermore, requiring only a single pass through the model, compared to more than 100 iterations for ControlNet.

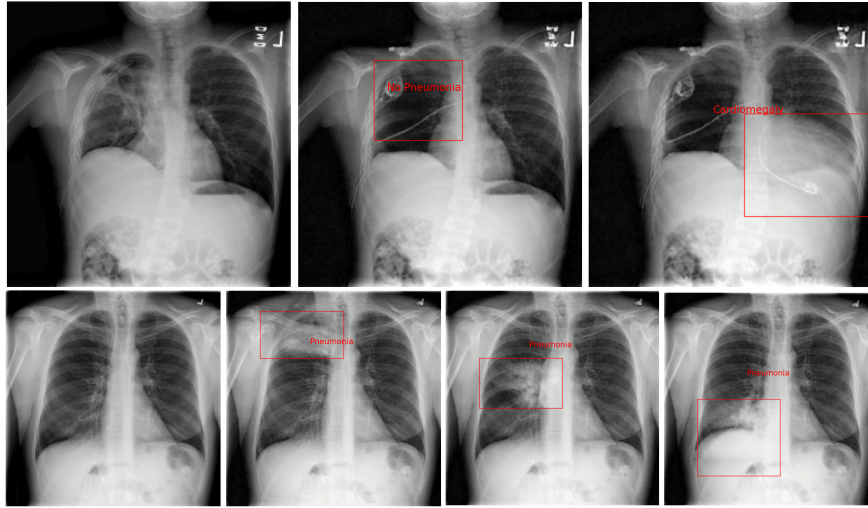


Fig. 3. Pathology infusion control with XReal. (top) XReal can be used for image editing, removing or adding any pathology from a given X-ray image. (bottom) Localized pathology infusion with XReal while keeping the anatomy intact.

Despite ControlNet’s lower FID score, its output shows inferior clinical realism based on the observed dice, SSIM, and F1 scores and expert radiologist evaluation. This strengthens our initial conjecture that FID is inadequate for medical realism assessment and should not be solely relied upon.

To further evaluate the clinical realism of the generated data, an expert radiologist with more than 16 years of experience reviewed the generated images. Since pathology annotations are unavailable in the MIMIC-CXR dataset, we utilize anatomy masks obtained from the anatomy segmentation model and pathology bounding boxes from the VinDr-CXR[26] dataset’s test set to generate images for radiologist evaluation. This expert evaluation test was conducted in a blind review setting, with the task to rank the generated images from all compared methods, XReal, ControlNet [40], Cheff [36] and RoentGen [6] along with the real images. The radiologist was asked to score images from 1 (lowest) to 5 (highest) based on anatomy realism and pathology manifestation in the correct location. As shown in 1, XReal outperformed other methods by a large margin with scores of 4.73 and 4.44 for anatomy and pathology, respectively, while notably surpassing the real image in both anatomy (4.12) and pathology realism (4.00) evaluation.

5 Discussion

XReal offers precise anatomy and pathology control while being lightweight, making it the first diffusion model to generate realistic X-ray images using

anatomy and pathology masks. ControlNet [40] model has been used in natural images, but no attempts have been made to train it for controllable X-ray generation. In this work, we trained ControlNet [40] on the same X-ray dataset, which performs poorly against our method in terms of anatomical control, but it also does not offer any spatial control over pathology manifestation, highlighting its shortcomings compared to our method. Fig. 1 shows how textual inputs do not perform as well as the direct spatial control regarding pathology manifestation. The report-to-xray models are limited in the control they provide over the spatial composition of the image, mainly due to the inherent ambiguity in the language itself. This limits their clinical applications, where more simulated and controlled images are required for training and planning.

We demonstrate the image editing capabilities of XReal in Fig. 3. XReal can seamlessly add or remove pathology from an X-ray, which has clinical significance, as it can be used for counterfactual image generation [8,15], disease prognosis, and simulation. XReal can also be used for training radiologists and primary patient education by generating the same X-ray with pathologies in different locations, as depicted in Fig. 3. This enables medical practitioners to visualize, analyze, and examine different cases of various diseases without the use of real data.

Using XReal, we generate and publicly release *BiomedCXR* dataset containing paired X-ray images, anatomy masks, and pathology annotations, which can have a positive impact on medical imaging research where such datasets are scarce. This dataset can be used to train robust models for classification, detection, segmentation, and explainability in X-ray images.

6 Conclusion

We introduce XReal, the first controllable diffusion model for realistic chest X-ray image generation through precise control over anatomy and pathology. XReal can edit a given X-ray image, simulating diverse clinical scenarios with varying anatomy and pathology. Through this, XReal can enable counterfactual generation, image editing, and disease simulation. Moreover, we generate and release a large X-ray dataset *BiomedCXR* containing paired anatomical masks, pathology annotation, and high-quality CXR images. A limitation of our work is the requirement of a separate diffusion backward process for anatomy and pathology control, which can be addressed in future work. Furthermore, we plan to extend this work to other modalities, including MRI and CT scans, where it can be used for various applications.

References

1. Alaluf, Y., Tov, et al.: Hyperstyle: Stylegan inversion with hypernetworks for real image editing. In: Proceedings of the IEEE/CVF CVPR (2022)
2. Avrahami, O., Hayes, T., Gafni, O., et al.: Spatext: Spatio-textual representation for controllable image generation. In: Proceedings of the IEEE/CVF Conference on Computer Vision and Pattern Recognition. pp. 18370–18380 (2023)

3. Brown, T., Mann, B., Ryder, N., et al.: Language models are few-shot learners. *Advances in neural information processing systems* **33** (2020)
4. Casanova, A., Careil, M., Romero-Soriano, A., et al.: Controllable image generation via collage representations. *arXiv preprint arXiv:2304.13722* (2023)
5. Chambon, P., Bluethgen, et al.: Adapting pretrained vision-language foundational models to medical imaging domains. *arXiv preprint arXiv:2210.04133* (2022)
6. Chambon, P., Bluethgen, C., Delbrouck, J.B., et al.: Roentgen: vision-language foundation model for chest x-ray generation. *arXiv preprint arXiv:2211.12737* (2022)
7. Ciano, G., Andreini, P., Mazzierli, T., et al.: A multi-stage gan for multi-organ chest x-ray image generation and segmentation. *Mathematics* (2021)
8. Cohen, J.P., Brooks, R., En, S., et al.: Gifsplanation via latent shift: a simple autoencoder approach to counterfactual generation for chest x-rays. In: *Medical Imaging with Deep Learning*. PMLR (2021)
9. Cohen, J.P., et al.: Torchxrayvision: A library of chest x-ray datasets and models. In: *International Conference on Medical Imaging with Deep Learning* (2022)
10. Couairon, G., Careil, M., Cord, M., et al.: Zero-shot spatial layout conditioning for text-to-image diffusion models. In: *Proceedings of the IEEE/CVF International Conference on Computer Vision* (2023)
11. Dhariwal, P., Nichol, A.: Diffusion models beat gans on image synthesis. *Advances in neural information processing systems* **34** (2021)
12. Dinh, T.M., Tran, A.T., Nguyen, R., et al.: Hyperinverter: Improving stylegan inversion via hypernetwork. In: *Proceedings of the IEEE/CVF Conference on Computer Vision and Pattern Recognition* (2022)
13. Dorjsembe, Z., Pao, H.K., Odonchimed, S., Xiao, F.: Conditional diffusion models for semantic 3d medical image synthesis. *arXiv preprint arXiv:2305.18453* (2023)
14. Goodfellow, I., Pouget-Abadie, J., Mirza, M., et al.: Generative adversarial nets. *Advances in neural information processing systems* **27** (2014)
15. Gu, Y., Yang, J., Usuyama, N., et al.: Biomedjourney: Counterfactual biomedical image generation by instruction-learning from multimodal patient journeys. *arXiv preprint arXiv:2310.10765* (2023)
16. Heusel, M., Ramsauer, H., Unterthiner, T., et al.: Gans trained by a two time-scale update rule converge to a local nash equilibrium. *Advances in neural information processing systems* **30** (2017)
17. Ho, J., Jain, A., Abbeel, P.: Denoising diffusion probabilistic models. *Advances in neural information processing systems* **33** (2020)
18. Huang, G., Liu, o.: Densely connected convolutional networks. In: *Proceedings of the IEEE conference on computer vision and pattern recognition* (2017)
19. Johnson, A., Pollard, T., Mark, R., et al.: Mimic-cxr database (version 2.0. 0). *physionet* (2019)
20. Kingma, D.P., Welling, M.: Auto-encoding variational bayes. *arXiv preprint arXiv:1312.6114* (2013)
21. Konz, N., Chen, Y., Dong, H., et al.: Anatomically-controllable medical image generation with segmentation-guided diffusion models. *arXiv preprint arXiv:2402.05210* (2024)
22. Kumar, A., Anand, K., Mandloi, S., et al.: Coronetgan: Controlled pruning of gans via hypernetworks. In: *Proceedings of the IEEE/CVF ICCV* (2023)
23. Liu, B., Yang, Z., Wang, P., et al.: Textdiff: Mask-guided residual diffusion models for scene text image super-resolution. *arXiv preprint arXiv:2308.06743* (2023)
24. Meng, C., et al.: SDEdit: Guided image synthesis and editing with stochastic differential equations. In: *International Conference on Learning Representations* (2022)

25. Ng, M.F., Hargreaves, C.A.: Generative adversarial networks for the synthesis of chest x-ray images. *Engineering Proceedings* **31**(1), 84 (2023)
26. Nguyen, H.Q., Lam, K., Le, L.T., et al.: Vindr-cxr: An open dataset of chest x-rays with radiologist's annotations. *Scientific Data* **9**(1) (2022)
27. Packhäuser, K., Folle, o.: Generation of anonymous chest radiographs using latent diffusion models for training thoracic abnormality classification systems. In: 2023 IEEE 20th International Symposium on Biomedical Imaging (ISBI). IEEE (2023)
28. Park, D.H., Luo, G., Toste, C., et al.: Shape-guided diffusion with inside-outside attention. In: *Proceedings of the IEEE/CVF Winter Conference on Applications of Computer Vision* (2024)
29. Paszke, A., Gross, S., Massa, F., et al.: Pytorch: An imperative style, high-performance deep learning library. *Advances in neural information processing systems* **32** (2019)
30. Ramesh, A., Dhariwal, P., Nichol, A., et al.: Hierarchical text-conditional image generation with clip latents. *arXiv preprint arXiv:2204.06125* (2022)
31. Rawte, V., Sheth, A., Das, A.: A survey of hallucination in large foundation models. *arXiv preprint arXiv:2309.05922* (2023)
32. Rombach, R., Blattmann, A., Lorenz, D., et al.: High-resolution image synthesis with latent diffusion models. In: *Proceedings of the IEEE/CVF CVPR* (2022)
33. Segal, B., Rubin, D.M., Rubin, G., Pantanowitz, A.: Evaluating the clinical realism of synthetic chest x-rays generated using progressively growing gans. *SN Computer Science* **2**(4), 321 (2021)
34. Stojanovski, D., Hermida, et al.: Echo from noise: Synthetic ultrasound image generation using diffusion models for real image segmentation. In: *Simplifying Medical Ultrasound*. pp. 34–43. Springer Nature Switzerland, Cham (2023)
35. Van, P.N., Minh, D.T., Huy, H.P., et al.: Echocardiography video synthesis from end diastolic semantic map via diffusion model. *arXiv preprint arXiv:2310.07131* (2023)
36. Weber, T., Ingrisch, M., Bischl, B., and others: Cascaded latent diffusion models for high-resolution chest x-ray synthesis. In: *Pacific-Asia Conference on Knowledge Discovery and Data Mining*. Springer (2023)
37. Xie, J., Li, Y., Huang, Y., et al.: Boxdiff: Text-to-image synthesis with training-free box-constrained diffusion. In: *Proceedings of the IEEE/CVF International Conference on Computer Vision* (2023)
38. Xie, S., Zhang, Z., Lin, Z., et al.: Smartbrush: Text and shape guided object inpainting with diffusion model. In: *Proceedings of the IEEE/CVF Conference on Computer Vision and Pattern Recognition* (2023)
39. Yang, X., Gireesh, N., Xing, E., et al.: Xraygan: Consistency-preserving generation of x-ray images from radiology reports. *arXiv preprint arXiv:2006.10552* (2020)
40. Zhang, Lvmin, o.: Adding conditional control to text-to-image diffusion models. In: *Proceedings of the IEEE/CVF International Conference on Computer Vision* (2023)

Appendix

A1 Algorithm

Algorithm 1 XReal inference process with anatomy and pathology control

Require: $\hat{x}_v \in \mathbb{R}^{3 \times 64 \times 64}$ ▷ Latent of \hat{x}
Require: $m \in \mathbb{R}^{3 \times 64 \times 64}$ ▷ Anatomy or Pathology Mask
Require: $s \in \mathbb{R}$ ▷ Number of steps to mask for
Require: p ▷ Pathology prompt
 $x_T \sim \mathcal{N}(0, I)$
for $t = T, \dots, 0$ **do**
 if $t \geq s$ **then**
 $\epsilon \sim \mathcal{N}(0, I)$
 $x_v^t = \sqrt{\alpha_t} \hat{x}_v + \sqrt{1 - \alpha_t} \epsilon$
 $x_t = m \cdot x_v^t + (1 - m) \cdot x_t$
 end if
 $z \sim \mathcal{N}(0, I)$ **if** $t > 1$ **else** $z = 0$
 $x_{t-1} = \frac{1}{\sqrt{\alpha_t}} (x_t - \frac{1 - \alpha_t}{\sqrt{1 - \alpha_t}} \epsilon_\theta(x_t, t, p)) + \sigma_t z$
end for
return x_0

A2 Generated Images

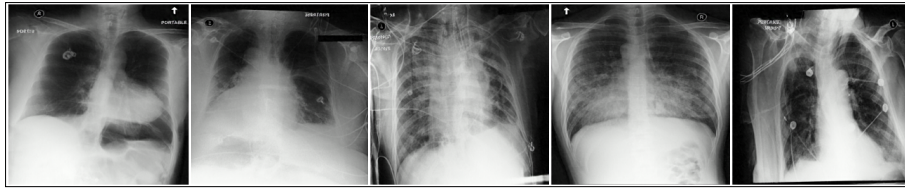


Fig. A2.1. Image with high artefact (e.g. heart at the wrong location) generated during one of the experiments can achieve low FID score of ~ 30 . This shows that the FID score does not regard realism and merely compares the distribution of two datasets, making it unsuitable for medical applications.

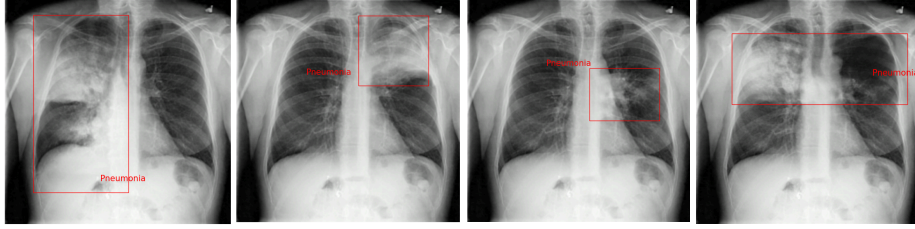


Fig. A2.2. XReal provides precise control over pathology manifestation while preserving image quality. Demonstrating varying pneumonia severity in different image regions can aid medical research, diagnosis, and treatment planning, enhancing understanding and patient care.

Prompt	Cheff	RoentGen	Prompt	Pathology Mask	XReal (ours)
An x-ray image with no cardiomegaly.					
An x-ray image with cardiomegaly.			cardiomegaly		
An x-ray image with pneumonia in the lower right lung.			pneumonia		

Fig. A2.3. Pathology infusion in a specific location using different diffusion models. Text-to-image methods (Cheff and RoentGen) fail to localize the specified pathology in the right location and struggle to incorporate the given prompt precisely. On the other hand, XReal can not generate an X-ray image with a given anatomy, but it can seamlessly infuse the specified lesion at the desired location.

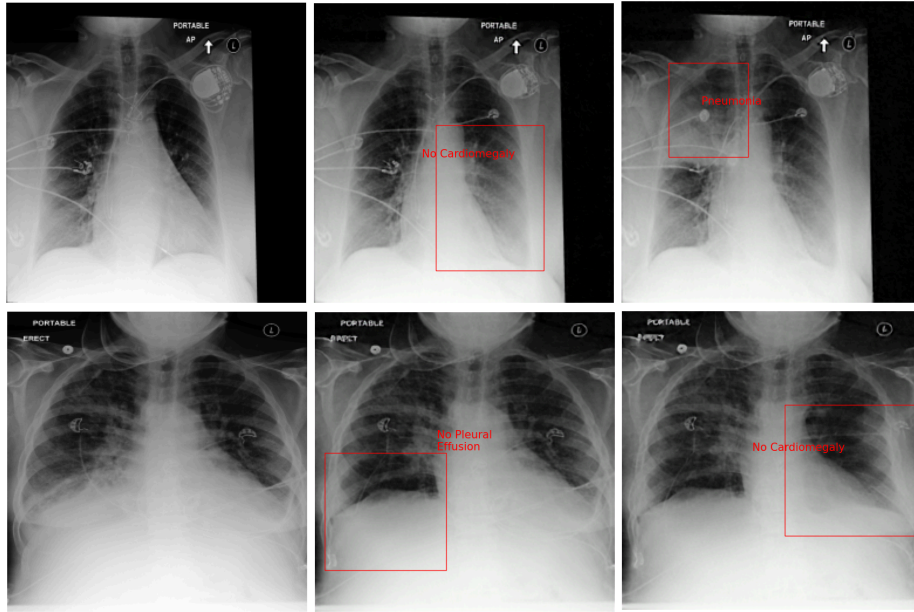


Fig. A2.4. XReal offers great control to add or remove pathology from a specific location in a given x-ray image. Here, we used three real X-ray images to demonstrate the pathology control provided by XReal, remove one pathology, and then add/remove another pathology, showcasing its utility in counterfactual generation and educational training.